Pergamon

Ann. occup. Hyg., Vol. 41, No. 1, pp. 105–122, 1997

Published by Elsevier Science Ltd. Printed in Great Britain
0003–4878/97 $17.00 + 0.00

PII: S0003–4878(96)00025–7

SPATIAL AND TEMPORAL VISUALIZATION OF GASES AND VAPOURS IN AIR USING COMPUTED TOMOGRAPHY. NUMERICAL STUDIES

Runa Bhattacharyya and L. A. Todd*

Department of Environmental Sciences and Engineering, University of North Carolina at Chapel Hill, CB 7400, Chapel Hill, NC 27599, U.S.A.

(*Received in final form* 23 *January* 1996)

Abstract—Numerical studies were performed to evaluate a new method for human exposure assessment and source monitoring, based upon optical remote sensing (ORS) and computed tomography (CT). With an ORS-CT system, two-dimensional maps of chemical concentrations in air, with good spatial and temporal resolution, can be created over a confined space such as a workplace room. The ORS-CT system was evaluated using 15 simulated test maps that model the generation and dispersion of contaminant plumes over time. A program simulated field measurements from these maps assuming different remote sensing scan times. Using these measurements, reconstructed maps were generated and compared with original maps. Qualitative and quantitative methods were used to evaluate the effect on reconstruction quality of sample time, number of iterations used by the maximum likelihood expectation maximization reconstruction algorithm and sample density. For this study, scanning an entire room in 10 min was adequate for exposure evaluation, source monitoring and leak detection.

NOMENCLATURE

a	Weighting factor representing the contribution of a grid cell to a raysum
c	Concentration of pollutant in a grid cell of the reconstructed map
c^*	Concentration of pollutant in a grid cell of the original test map
i	The number of infrared (IR) beams, varying from 1 to M
j	The number of grid cells in the reconstruction grid, varying from 1 to N^2
M	Total number of IR beams
N	Number of grid cells on any side of the square reconstruction grid
n	Number of iterations performed by the algorithm
p	Line integrated concentration or raysum along an IR beam
t_{ij}	Transfer matrix from image cell j to set of parallel projections i
x, x^*	x coordinate of the location of the peak in the reconstructed map, original test map
y, y^*	y coordinate of the location of the peak in the reconstructed map, original test map
θ	Projection angle

INTRODUCTION

Conventional air sampling devices used for human exposure assessment or source monitoring produce integrated or real-time measurements which have limited spatial and temporal resolution. These measurements are restricted to a limited number of

*Author to whom correspondence should be addressed.

individuals or areas in a room and, therefore, are used to infer exposures for a larger workforce or the unsampled areas in a room. These inferences may not be defensible. Integrated measurements typically smooth out fluctuations in concentrations; thus, acute exposures or short-term source emissions cannot be readily resolved.

A new air sampling technology has been proposed which creates two-dimensional maps of contaminants to provide accurate spatial and temporal information about contaminant concentration and flow (Todd and Leith, 1990). This technology combines the measurement techniques of optical remote sensing (ORS) with the mapping capabilities of computed tomography (CT). While any open-path system could conceivably be used for tomography, this research uses open-path Fourier transform infrared (OP-FTIR) spectrometers to scan the air and detect, *in situ* and in real-time, a wide variety of contaminants of interest to the industrial hygienist, at concentrations down to a few parts per million (Strang and Levine, 1989). Each single beam of infrared (IR) light probes the air, measuring the attenuation of light from peripherally placed optical sources or retroreflectors, and provides line-integrated contaminant concentrations along the path of the beam through the room. When a network of intersecting line-integrated concentrations is obtained, tomographic algorithms are used to transform the set of concentrations into a spatially resolved, two-dimensional concentration map, along the plane sampled. These maps are then linked together to visualize spatial and temporal changes in concentrations and chemical species in a room. The level of concentration detail provided by these maps requires far fewer measurements to obtain the same level of detail than would be required using conventional point sampling methods. An ORS-CT system may enable near real-time evaluations of short-term or chronic peak exposures, at any location in a measurement space, and provide a tool to determine ventilation efficiency and pollutant transport (Yost *et al.*, 1994).

The introduction and development of this ORS-CT technology was described in previous papers which used numerical studies to evaluate ORS-CT configurations (location and number of OP-FTIR spectrometers) and tomographic reconstruction algorithms (Todd and Leith, 1990; Todd and Ramachandran, 1994a,b), and experimental studies to evaluate this method in an exposure chamber (Yost *et al.*, 1994; Samanta and Todd, 1994). While the numerical studies demonstrated the feasibility of using an ORS-CT system for achieving good spatial resolution, they did not consider temporal resolution. The experimental studies had promising results but hardware limitations compromised the temporal resolution.

One of the greatest challenges facing implementation of a tomographic system is reconstructing an image that is not stationary. In the workplace, this relates to characterizing spatially changing concentration profiles. To obtain a network of open-path measurements, each OP-FTIR spectrometer sequentially scans the air and each measurement is taken at a different point in time. This introduces inconsistencies in the data which will adversely affect reconstruction accuracy. The total time required to completely sample an area depends upon the number of OP-FTIR light beams and spectrophotometers, and the time required to obtain each individual open-path measurement. To map concentration profiles in the flux accurately, the time required to sample the entire room must be balanced with the movement of air contaminants.

This paper reports on numerical studies that evaluated the ability of an ORS-CT system to reconstruct maps from changing concentration profiles. The investigation examined the effect on reconstruction quality of interferometer scan time, measurement noise and number density of rays.

THEORY AND METHODOLOGY

Computed tomography

As applied to air monitoring, computed tomography is the process of measuring a spatial concentration profile of a plane through a room, using a network of line-integrated concentration data. The computations transform one-dimensional measurements of a concentration to a two-dimensional estimate of concentrations using another two-dimensional function (Herman, 1980). A network of OP-FTIR light beams are shot through the plane into the area to be monitored to obtain line-integrated gas concentrations (or raysums). The number and angular location of the rays in the network comprise the remote sensing configuration. Raysums obtained with the configuration are then used by tomographic algorithms to reconstruct maps. The strategy is to obtain concentrations in the reconstructed map which would most likely yield the same line-integrated concentrations as those obtained from the measured raysum data (Herman, 1980).

The idealized measurement space is broken into an $N \times N$ grid of cells. Figure 1 shows a 10×10 grid of 100 cells. Each cell, j, is assigned a concentration c_j, which is assumed to be uniform and non-negative. Raysums are line integrals of c_j along various paths through the room. The acute angle that an IR beam makes with the room side is called the projection angle, and the ith ray sum is p_i. The rays have a finite width and, therefore, are approximated by strip sums. The relationship between cell concentrations and raysums can be expressed as

$$p_i = \Sigma a_{ij} c_j,\ i = 1 \ldots M, j = 1 \ldots N^2, \tag{1}$$

where p_i is the raysum at projection angle θ, a_{ij} is the weighting factor representing the contribution of jth cell to the ith raysum, M is the total number of rays, i is the number of the ray, ranging from 1 to M and N^2 is the total number of cells in an $N \times N$ grid. For the numerical studies, time series concentration maps were generated from dispersion models to simulate spatial concentration changes over time. Raysums were computed then from the time series concentration maps using a simulated four source scanning configuration. The raysums were used by an iterative reconstruction algorithm in simulations performed to evaluate the effect of timestep (measurement time), measurement noise, number of iterations used by the algorithm and sampling density. The reconstructed concentration maps were then compared with the original maps to evaluate reconstruction quality.

Test concentration maps

Fifteen different sets of temporally changing test concentration profiles were generated using a two-dimensional advection diffusion equation with a bi-variate Gaussian source (Hanna *et al.*, 1982). Source emission rate, diffusion coefficient, air velocity, source location, source intensity and standard deviation of the Gaussian

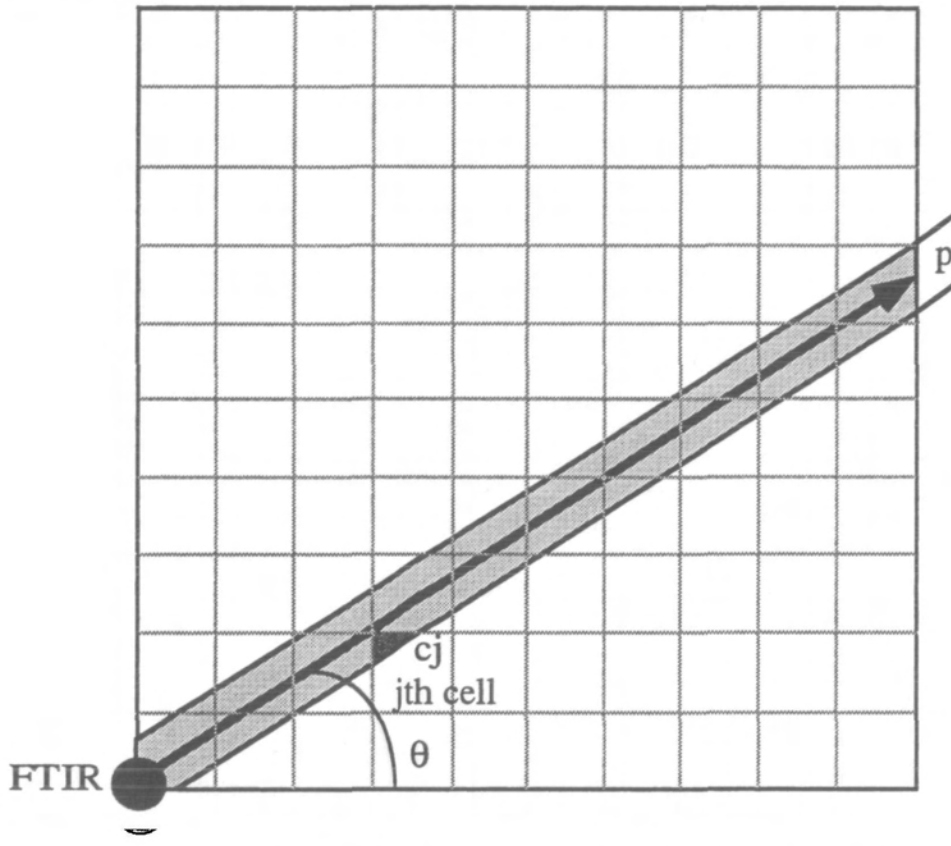

Fig. 1. Geometry of reconstruction on a 10×10 grid with 100 cells. The projected ray sum, p_i, with a projection angle of q. The concentration of the contaminant in the jth cell is c_j.

source were varied to obtain the test maps (ACGIH, 1995; 3M-OHESD, 1992). The hypothetical cross-section of the room was broken into a 40×40 grid of cells. For each set of test maps, a time series of original maps was created, with each map reflecting the spatial change in concentrations in the grid of cells after 15 s. Thus, a set of 720 maps was obtained to represent a time frame of 3 h.

Table 1 lists the time series concentration maps, and Fig. 2 represents some sample test maps. Six sets of time series maps represent the generation or decay of a single contaminant source in rooms with relatively still air (time series 1–5), and with air velocity rates that vary up to $1\ m\ s^{-1}$ (time series 6, 7, 11, 12). The higher the air velocity the greater the spatial displacement of the peaks over time. To test the limits of the parameters modelled in this study, time series 12 has a very sharp concentration peak with a logarithmic rate of decay. To isolate the effect of spatial movement of contaminants from changes in concentration when there is little movement, three sets of time series maps (8, 9, 10) were artificially created by modifying maps discussed above. Thus, for time series 9 and 10, time series 1 and 3, respectively, were modified to change the dispersion rates (movement) of a decaying peak artificially. For time series 8, time series 1 was modified to change the dispersion rates (movement) of a steady state peak artificially. Three sets of time

Table 1. Numerical simulations performed

Series	Test concentration maps	Timestep	Noise	150 iterations	No. of Rays 80,30,20
1	Peak at side, decay	1–12	1–4		1–4
2	Peak at side, generation	1–12	1–4		
3	Peak at middle, decay	1–12		1–4	
4	Peak at middle, generation	1–12		1–4	
5	Peak at middle, slow decay	1–8			
6	Peak moving, generation	1–12	1–4	1–4	1–4
7	Peak moving, slow generation	1–8	1–4		1–4
8	Peak moving, no other change	1–12			
9	Series 1 modified to move at the same rate as Series 7	1–4			
10	Series 3 modified to move faster than Series 7	1–4			
11	Peak moving, generation	1–4			
12	Gas release scenario	1–8	1–4	1–4	
13	Two peaks	1–4			
14	Three peaks	1–4			
15	Four peaks	1–4	1–12		

The first two columns list the 15 sets of time series maps generated and their general properties. The third column lists the range of timestep values for which CT reconstructions were calculated, using a baseline of 40 rays per OP-FTIR scanner, no measurement noise and 50 iterations. The fourth, fifth and sixth columns list the range of timestep values for which CT reconstructions were calculated, using noise, 150 iterations, and 20, 30 and 40 rays, respectively.

series maps represent the generation or decay of multiple contaminant sources in rooms (13–15).

Remote sensing configuration

A symmetrical, non-invasive remote sensing configuration was simulated which used four OP-FTIR spectrometers, one in each corner of a 40×40 room, that simultaneously scanned the room (see Fig. 3). Each OP-FTIR spectrometer sends a beam of infrared (IR) light across the room to a corner cube retroreflector, which then returns the beam directly back to its point of origin. The spectrometer then sequentially rotates to a new position, sends out another beam of IR light and obtains another measurement. The basic configuration used 40 rays per OP-FTIR spectrometer; this resulted in a well sampled room with a network of relatively orthogonal rays (Todd and Ramachandran, 1994a,b).

Reconstruction algorithm

An iterative tomographic reconstruction algorithm, maximum likelihood with expectation maximization (MLEM), was chosen for this study. This simultaneous iteration technique, corrects all cells at once after an entire set of raysum data is obtained in each iteration (Tsui *et al.*, 1991; Shepp and Vardi, 1982), as shown in Equation (2):

$$C_j^{(n+1)} = (c_j^n / \Sigma t_{ij}) * \Sigma(t_{ij} p_i / \Sigma t_{ij} c_j^n), \tag{2}$$

where $C_j^{(n+1)}$ = concentration in jth cell after the nth iteration, $\Sigma t_{ij} c_j^n$ = re-projection of the image estimate c_j^n and $\Sigma t_{ij} p_i$ = backprojection of the projection array.

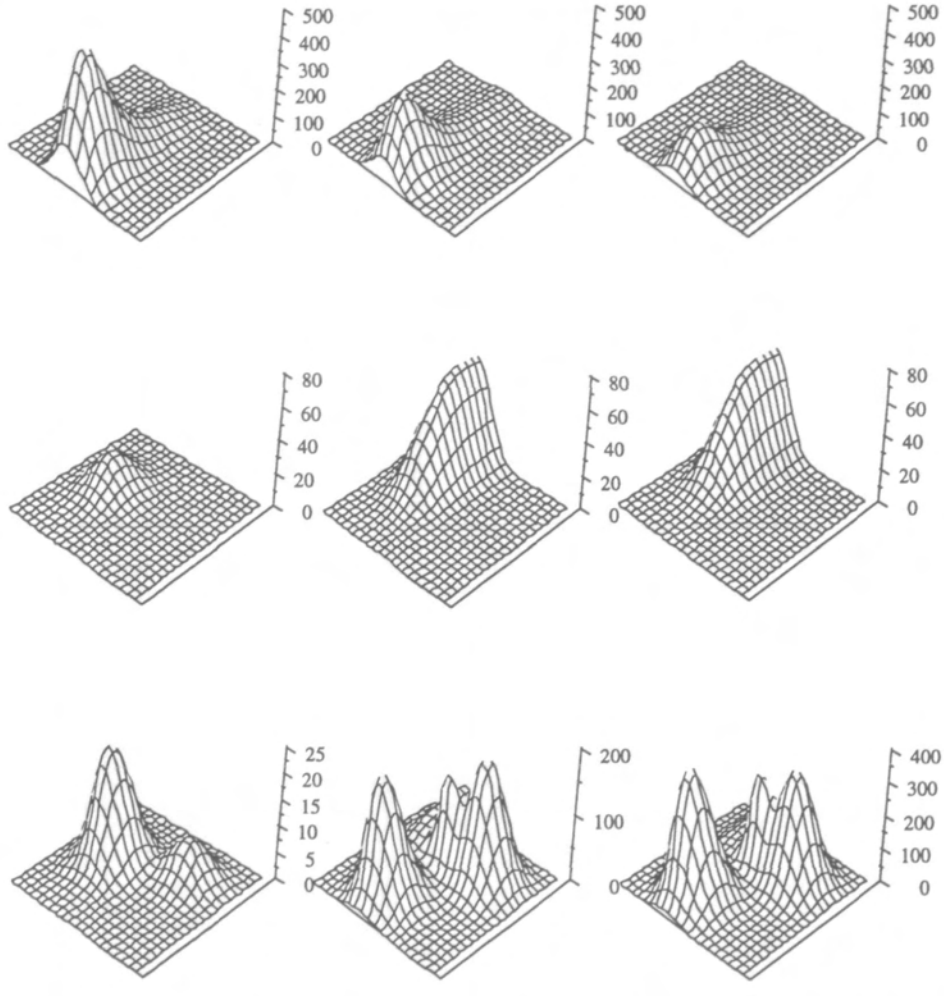

Fig. 2. Some representative test concentration profiles, 15 s, 1.5 h and 3 h after starting to take measurements. (a) Decay of single contaminant source (time series 1); (b) generation of a pollutant with an air velocity of 0.3 m s^{-1} (time series 11); (c) generation and decay of four contaminant sources (time series 15).

The concentration distribution is estimated by using the maximum likelihood criterion which is given by Equation (3):

$$\ln L(C) = \Sigma - \Sigma t_{ij} c_j + p_i \ln(\Sigma t_{ij} c_j) - \ln(p_i), \tag{3}$$

where $L(C)$ is the likelihood of generating the image C, t_{ij} is the transfer matrix from image cell j to set of parallel projections i, c_j is the concentration at cell j, p_i is the raysum for the ith set of projections, i is the number of rays, 1 to M, and j is the number of cells, 1 to N^2. The likelihood strictly increases at each step unless it is at a maximum; therefore, all the cells have positive values of concentration.

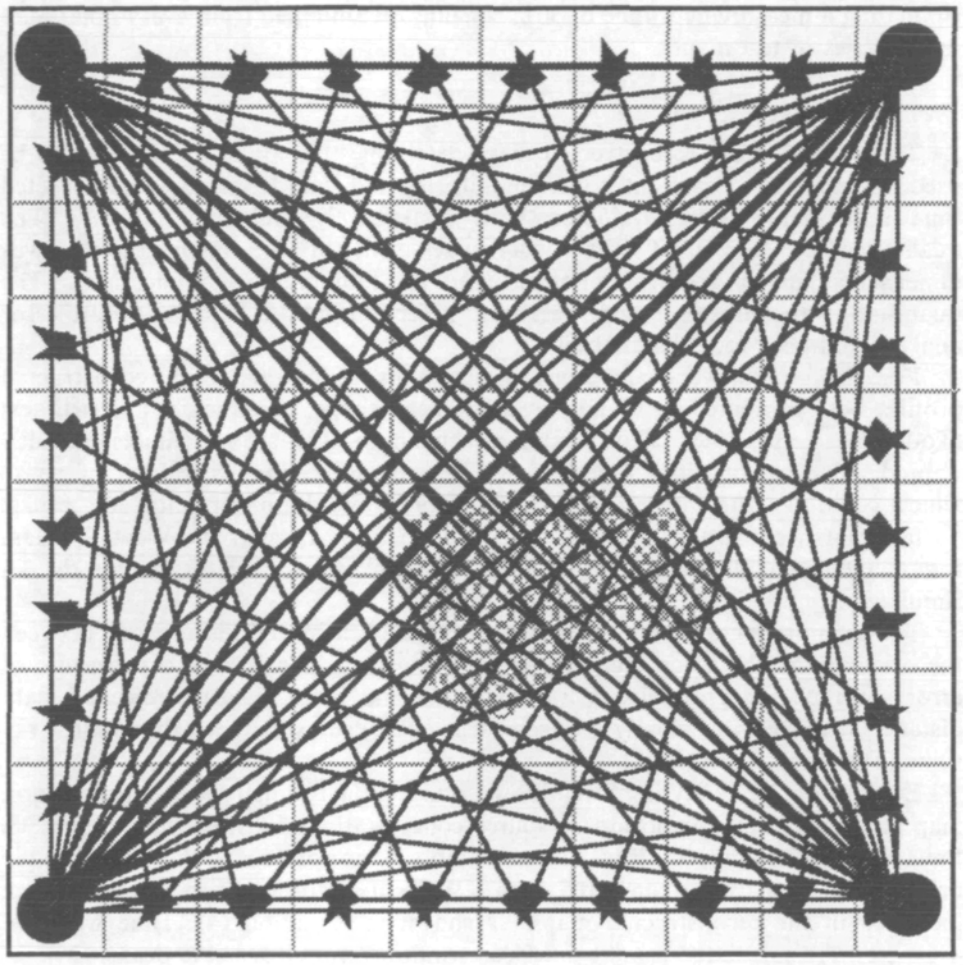

Fig. 3. Basic configuration of OP-FTIR scanners. The OP-FTIR scanners are represented by circles, one in each of the corners of the room. The arrows represent open-path infrared beams.

Timestep

The time required to obtain each line-integrated measurement was varied from a minimum of 15 s (timestep 1) to a maximum of 3 min (timestep 12). Using the basic configuration, this translates into the entire room being sampled once every 10 min to 2 h. A timestep of 1 implies that each OP-FTIR spectrometer measurement is taken at the same rate as the rate of change of each test concentration map. Thus, for a timestep of 1, the first set of raysums (four raysums, one from each OP-FTIR spectrometer) is taken from the first map in the series of test maps; the remaining sets of raysums are sequentially obtained from subsequent maps. When the entire set of 40 raysums per OP-FTIR spectrometer is obtained, the first reconstruction is performed and a tomographic map generated. After this point, tomographic maps are created after each set of raysums is obtained; this yields a total of 680 reconstructed maps from the 720 sets of measurements. For a timestep of 2,

simulating a measurement time of 30 s, raysums are obtained from every other map in the series of test maps.

Evaluating reconstruction quality

The quality of the reconstructed maps determines the ability of the map to be used for exposure assessment, source monitoring and leak detection. Reconstructed time series maps were evaluated both qualitatively and quantitatively. The qualitative measure used was visual assessment of the reconstructed two-dimensional maps and is important for all tomographic applications. The quantitative measures used were nearness, projection data distance, exposure error analysis and peak location analysis.

For the qualitative evaluation, surface plots of original and reconstructed profiles were compared to visually evaluate peak shape, peak height and artifacts (Todd and Leith, 1990; Todd and Ramachandran, 1994a,b). Artifacts included unpredictable irregularities that looked like salt and pepper, streaking of peaks which could be attributed to the configuration, and false concentration peaks. Surface plots were visualized using Spyglass Transform, Format and View (Spyglass Inc., Champaign, Illinois, U.S.A.). Maps were linked together to animate the 3 h simulated sample time.

The quantitative measure nearness reflects the cell-by-cell discrepancy between the original and the reconstructed concentration map, and is a global measure of errors over all the grid cells in a map (Todd and Leith, 1990). Projection data distance measures how closely the reconstructed ray sums matched the original ray sums (Todd and Leith, 1990).

Exposure error analysis reflects how accurately a reconstructed concentration map measures human exposure or source concentration. In these simulations, 3 h time weighted average (TWA) concentrations for exposures at the peaks in the original test map, were compared with TWA concentrations for the same peak locations in the reconstructed maps, as shown in Equation (4). Time weighted averages were calculated using a 5×5 cell window centred over the peaks.

$$\text{TWA Exposure Error} = -\frac{\sum_{\text{time}} \sum_{\text{space}} c_j^* - \sum_{\text{time}} \sum_{\text{space}} c_j}{\sum_{\text{time}} \sum_{\text{space}} c_j^*} \times 100, \qquad (4)$$

where time varies from the first time series map to the 720th map, space represents the 5×5 cell window around a peak, c_j^* is the concentration of the jth cell in the test map and c_j is the concentration in the jth cell in the reconstructed map. Peak location error describes how accurately a reconstructed map can pinpoint the location of an emission source and is important for leak detection. Peak error is the root mean square (RMS) difference in the location of the peak in the original and reconstructed map, as shown in Equation (5).

$$\text{Peak Location Error} = x - x^{*2} + y - y^{*2}, \qquad (5)$$

where x is the x coordinate of the location of the peak in the reconstructed image, x^* is the x coordinate of the location of the peak in the test map, y is the y coordinate of the location of the peak in the reconstructed image and y^* is the y coordinate of the location of the peak in the test map.

Simulated sampling parameters

To establish a baseline, all 15 time series maps were tested under ideal sampling conditions (no measurement noise), using 40 rays per OP-FTIR spectrometer, and were reconstructed using 50 iterations of the MLEM algorithm.

To investigate the effect on map quality of sampling density and sampling time, 30, 40 and 80 rays per OP-FTIR spectrometer were used for three representative time series maps (1, 6 and 7), for timesteps of 1 to 4. Thus, this resulted in sampling times for the entire room at a timestep of 1 of 7.5, 10 and 20 min for sampling densities of 30, 40 and 80 rays per OP-FTIR, respectively.

Measurement noise was simulated by adding random errors from a Gaussian distribution with a mean of zero and a standard deviation of 10 to the initial raysums for six representative time series maps (1, 2, 6, 7, 12 and 15) (Todd and Ramachandran, 1994a,b). For each test map, five simulations were performed in the presence of noise.

To evaluate the effect of number of iterations on map quality, reconstructions were performed using 50 iterations (time series 1–15) and 150 iterations (time series 3, 4, 6 and 12).

RESULTS AND DISCUSSION

Timestep

For all reconstructions of time series maps, as timestep increased (time required to obtain an open-path measurement), nearness, TWA exposure error, peak location error and data distance increased (deteriorated). Nearness was the most sensitive parameter to changes in timestep; data distance results were similar to nearness results. Figure 4 is plot of nearness versus timestep for three representative time series maps (1, 6 and 15). Below a timestep of 4, reconstructions from maps with multiple peaks resulted in higher (worse) nearness values than maps that primarily change concentration or have large spatial movements of peaks. At higher timesteps, however, large spatial changes resulted in the highest (worst) nearness values.

The impact of timestep on TWA exposure error is demonstrated in Fig. 5. At a timestep of 1, TWA exposures varied from being overestimated by an average of 8% to being underestimated by an average of 12%. For peaks which decayed over time (1, 3, 5–7, 9, 10, 13), timesteps of 1, 2 or 4 were best for exposure evaluation. A timestep of 1 overestimated exposure by an average of 8% while a timestep of 4 underestimated exposure by an average of 6%. For peaks which increased in concentration over time (2, 4, 11), timesteps of 1 were best for exposure evaluation. A timestep of 1 underestimated exposure by an average of 12% while a timestep of 4 underestimated exposure by an average of 17%. For time series maps with multiple peaks (13–15), TWA exposure error was relatively insensitive to increases in timestep, with errors varying from 11% overestimation to 30% underestimation. For timesteps 6 and above, TWA exposure errors varied from 30% to over 100% underestimation.

The two primary factors affecting underestimation or overestimation of TWA exposure error are whether peak concentrations are increasing or decreasing over time, and the inherent tendency of the reconstruction algorithm to smooth out

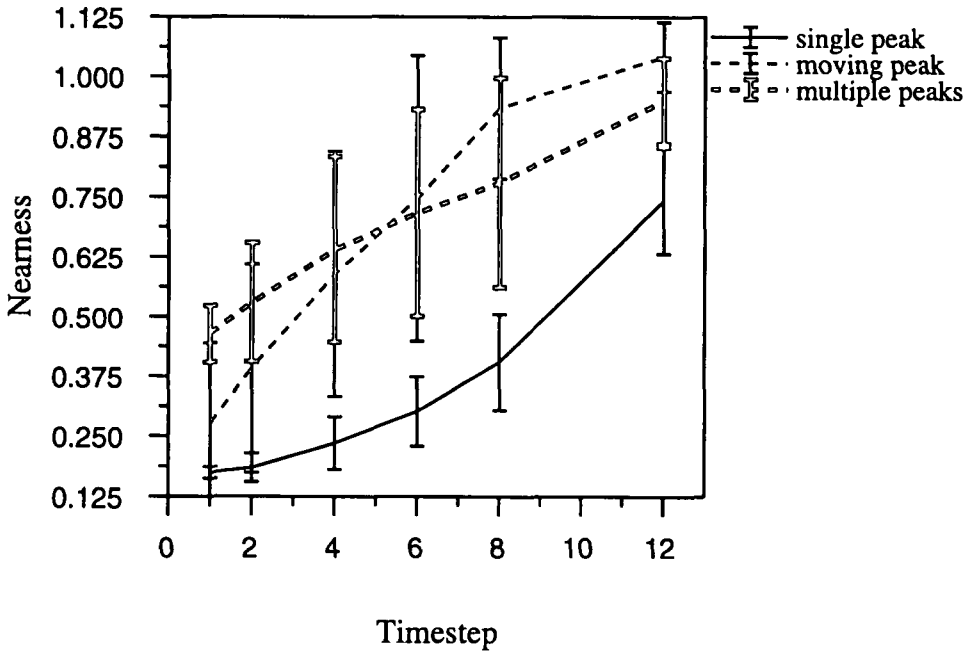

Fig. 4. Variation of nearness with timestep for three different sets of test concentration maps: time series 1, 6 and 15. The data points for nearness are an average of the nearness values obtained from each reconstructed map. Error bars represent one standard error.

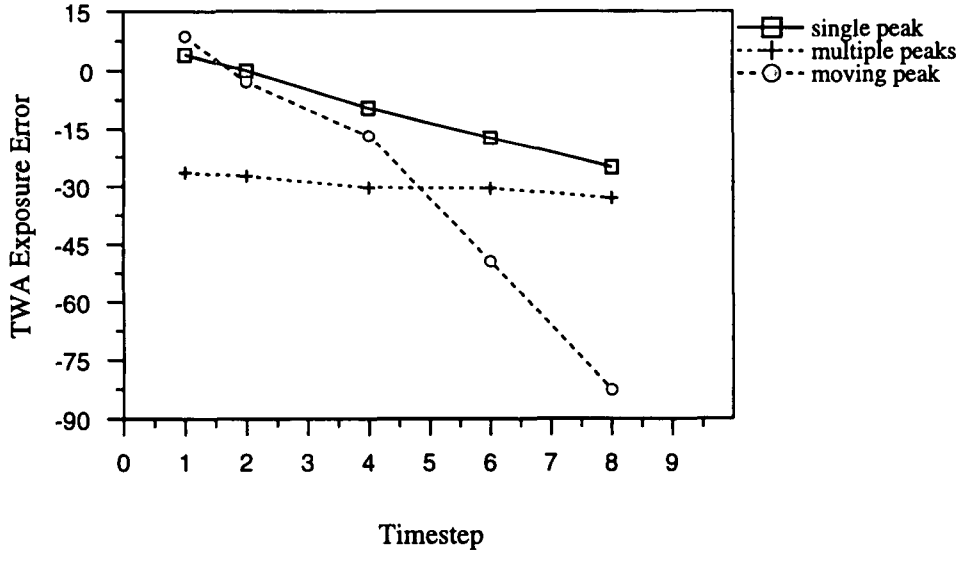

Fig. 5. Variation of TWA exposure error with timestep for three different time series sets of test concentration maps: time series 1, 6 and 15.

images and lower peak heights. When maps are reconstructed, raysums from previous time periods are used to reconstruct the current concentration profile. If concentrations are decreasing, older raysums will contain higher concentrations which may result in overestimation of peak heights. Similarly, if concentrations are increasing, older raysums will contain lower concentrations which will result in reconstructions that underestimate peak heights.

Peak location error, which indicates how far a concentration peak is reconstructed relative to its original location, was fairly insensitive to increases in timestep, particularly above a timestep of 4; see Fig. 6. For all the time series maps, the mean peak location error varied from 0 to 2, for a timestep of 1, and 0 to 14 (mean of 9.78) for a timestep of 8. For the time series maps which had single or multiple peaks, even at a timestep of 8, the peak location was pinpointed to within two cells; this is equivalent to a distance of 2 m for a 40 m^2 room. The time series maps with the greatest spatial movement of concentration profiles had the highest (worst) peak location errors. Location error for a moving peak was twice as high as that for a rapidly decreasing peak with errors as high as 14 for the moving peak at timesteps greater than 4.

For all the time series maps, the reconstructed maps were in close appearance to the original maps for timesteps of 1 and 2; timestep 1 always resulted in the best reconstructions. For most of the maps, timestep 4 resulted in reconstructions with peaks that were identifiable in overall shape and location; however, there were additional false peaks, smearing of peaks, and salt and pepper artifacts. For timesteps higher than 4, important features of the profiles were lost in the reconstructions; most of the peaks were smeared across the map and configuration artifacts were present. Using one of the time series maps as an example, Fig. 7 shows

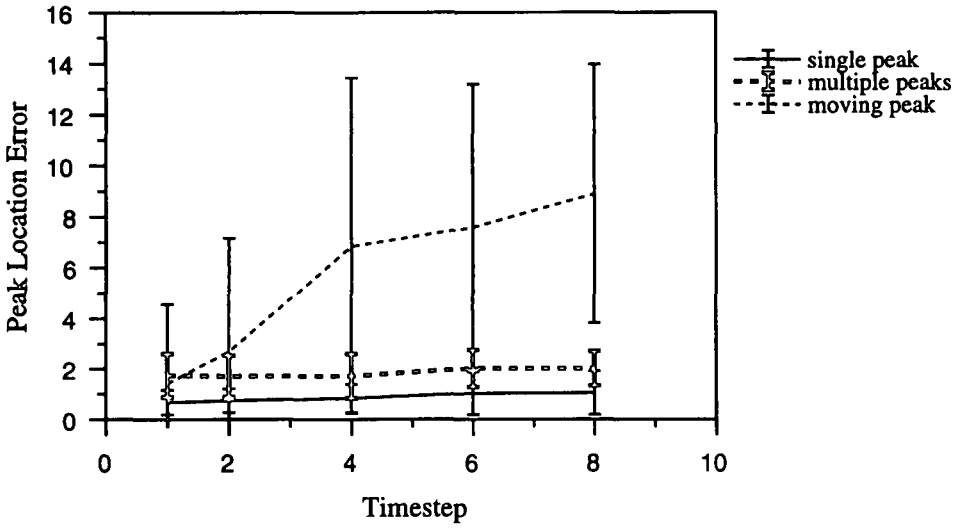

Fig. 6. Variation of peak location error with timestep for three different sets of test concentration maps: time series 1, 6 and 15. The data points for peak location error are an average of the values obtained from each reconstructed map. Error bars represent one standard error.

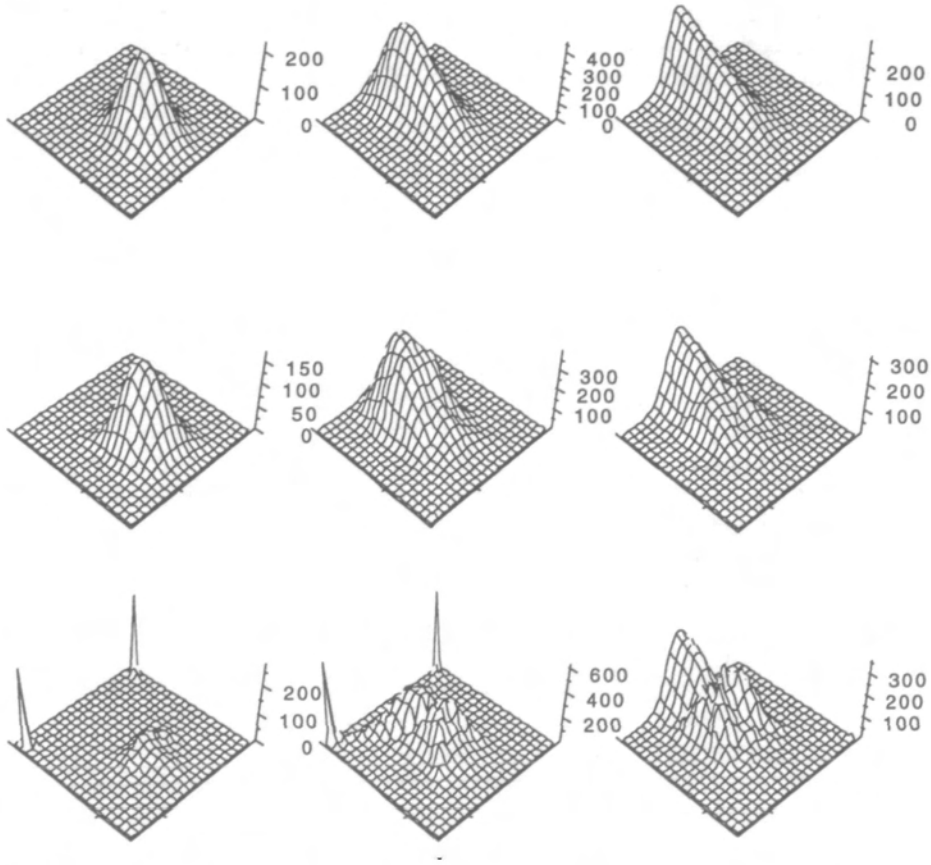

Fig. 7. Original and reconstructed test maps at timesteps of 1 and 4 after 40, 90 and 180 min. (a) Original test map (time series 6); (b) reconstructions at a timestep of 1; (c) reconstructions at a timestep of 4.

reconstructions from time series map 6, at a timestep of 1 and 4. Reconstructions at a timestep of 1 have peak shapes that are close in appearance to the original maps, and there are not many artifacts in the reconstructed maps. At a timestep of 4, the peak heights are considerably shortened, the reconstructions have salt and pepper artifacts, and peaks are smeared along the diagonal rays of the configuration, and there are false peaks in some corners. The relative differences in the reconstructions in Fig. 7, for different timesteps, are representative of the other time series maps as well.

The importance of visual evaluation was underscored in the multiple peak maps. While the TWA exposures were relatively constant over all the timesteps, visual evaluation revealed that there was a significant difference in peak heights between reconstructions at a timestep of 1 relative to a timestep of 4 or higher; at these higher timesteps most maps had artifacts, peaks were significantly shortened in height and peaks with lower concentrations were difficult to identify.

To test the limits of tomography, reconstructions from a simulated indoor gas release scenario as modelled by a rapidly decreasing peak were evaluated. Figure 8

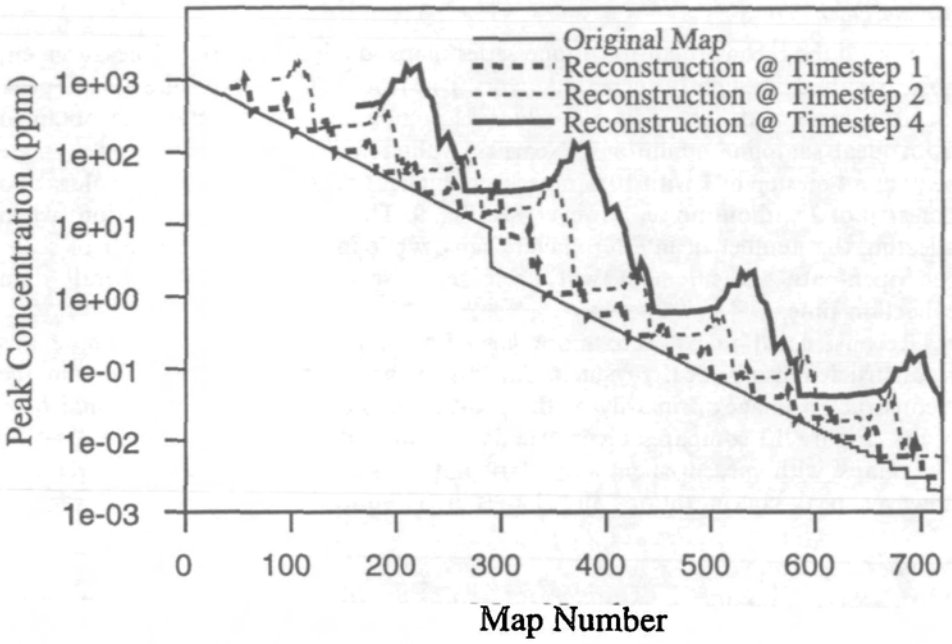

Fig. 8. Rate of decay of peak concentration for an indoor gas release scenario. Each map number represents 15 s of time.

shows the decay of peak concentration over time, represented by map number, for the original map and reconstructed maps at timesteps of 1, 2 and 4. The rate of change assumes a logarithmic profile, with concentrations dropping an order of a magnitude in 35 min. As shown in Fig. 8, peak height is overestimated significantly in the reconstructed images; the higher the timestep the greater the overestimation. Nearness values were very high, even at a timestep of 1. Based upon data distance values, reconstructed images were close to convergence at all timesteps. Mean peak location errors varied between 2 and 5 for timesteps of 1 and 4, respectively, suggesting that the proposed ORS-CT system is adequate for leak detection. Visual inspection of the images showed that while the shape and location of the concentration peak was well defined, the concentrations were significantly overestimated. This simulation assumes that the fastest time to scan a room is 10 min; therefore, this will be too slow to reconstruct concentrations accurately for a profile that changes rapidly; faster scanning will be necessary to evaluate such decay rates (Rasouli and Williams, 1995).

The cyclical pattern of the variation in peak height over time for the reconstructed map, seen in Fig. 8, is due to the configuration, or sequence in which raysums are collected when sampling maps with a single peak. Cyclical variations are not seen when spatial variation is high, or for test maps with multiple peaks. When the ray sums pass through the peak, these raysums contain the most recent information on concentration; therefore, reconstruction quality improves. When the ray sums pass through an area with little information content (concentration data), reconstruction quality deteriorates.

Measurement noise

For all the reconstructions of time series maps, the introduction of measurement noise resulted in slightly increased (worse) nearness, TWA exposure error, peak location error and data distance values as compared with the statistics obtained from ideal sampling conditions. Nearness values for reconstructions for a single peak at a timestep of 1 with 10% noise were higher (worse) than nearness values at a timestep of 2 without noise, however; see Fig. 9. This could have implications when selecting the number of interferometer scans; while increasing the number of scans per open-path measurement will decrease noise, it will increase overall data collection time.

Reconstructed maps were more jagged in appearance relative to the maps reconstructed using ideal raysums. Salt and pepper artifacts were evident in the reconstructed images primarily at the peaks, and some maps had additional false peaks. Figure 10 compares reconstructions with and without measurement noise. The maps with measurement noise are not as smooth as those without noise; however, peak concentrations and shapes are close to the ideal case.

Number of iterations

For ideal sampling conditions, there was no significant difference ($P > 0.05$) between reconstructions using 50 and 150 iterations of MLEM, but when 150

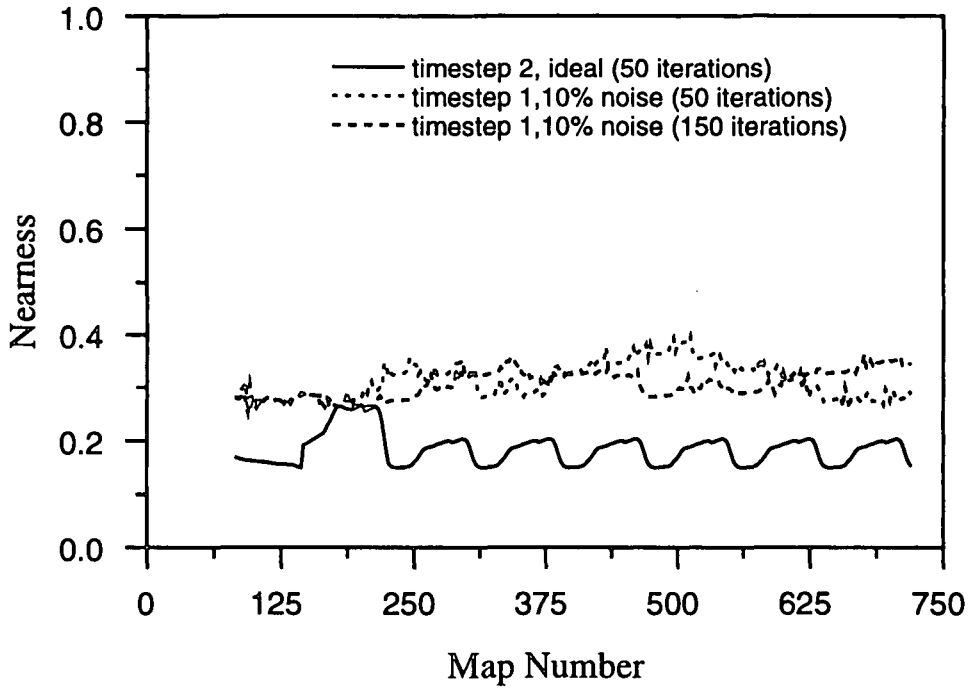

Fig. 9. Comparison of nearness from reconstructions of a single concentration peak at the side of a room at a timestep of 1 with 10% noise using 50 and 150 iterations of MLEM and a timestep of 2 with ideal measurements for 50 iterations of MLEM.

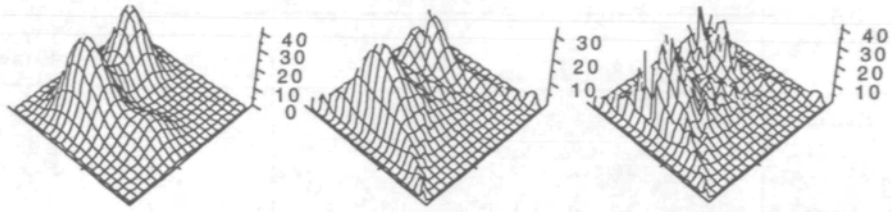

Fig. 10. Original and reconstructed test maps at a timestep of 1 reconstructed with 10% noise. (a) Original test map (time series 15); (b) reconstructed test map under ideal sampling conditions; (c) reconstructed test map with 10% measurement noise.

iterations were used to reconstruct maps containing ±10% measurement noise, both qualitative and quantitative image quality parameters improved. This improvement increased with increasing timestep. The effect of increased iterations in reconstructing a single peak with noisy data at a timestep of 1 is demonstrated in Fig. 9. There is no significant difference between noise and ideal nearness values at a timestep of 1 ($P=0.05$). However, for higher timesteps, there was a significant ($P<0.0001$) difference in nearness, data distance and TWA exposure errors. Inconsistency in raysum data due to temporal variations was more pronounced for higher timesteps and was enhanced by noise; therefore, a larger number of iterations were needed to achieve convergence.

Maps reconstructed using 150 iterations with and without noisy measurements resulted in smoother shapes of peaks than obtained from 50 iterations; however, information pertaining to peak location and shape of the image did not change. The computation time for 150 iterations is only 170% higher than that for 50 iterations (16 min for 150 iterations vs 6 min for 50 iterations for reconstructing 120 maps) on a Macintosh Quadra 650, which is insignificant in comparison to the time required for data collection.

Sampling density

An alternative to decreasing measurement time by reducing interferometer scan time is to use fewer open-path rays. When 30, 40, or 80 rays per OP-FTIR spectrometer were used to scan a room, the smaller the number density of rays, the lower (better) the nearness, data distance and TWA exposure errors. Figure 11 shows the nearness versus timestep when 30, 40 or 80 rays per OP-FTIR spectrometer were used to scan a room. When using 30 rays, TWA exposure error decreased (improved) by 13% over 40 rays. The reconstructions using 30, 40 and 80 rays were very similar to each other visually; however, peak heights for reconstructions using 30 rays were closer to the original map than reconstructions using 40 or 80 rays. These simulations indicate that coarser sampling may be a better means of tracking changing concentration profiles over time than using lower timesteps with finer sampling, but the peaks in these simulations were fairly broad and covered a relatively large spatial area. Sparser sampling may adversely impact the reconstruction of profiles with sharper peaks than the maps studied in these simulations.

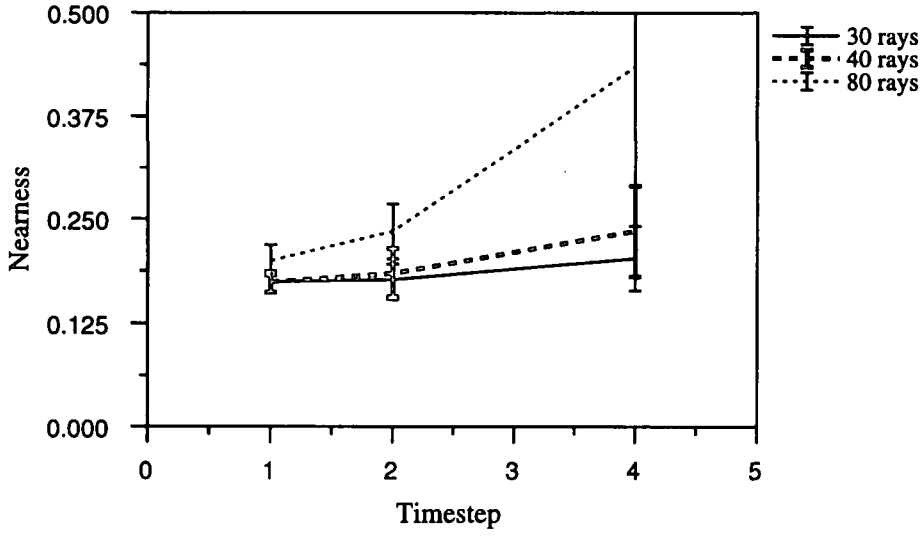

Fig. 11. Variation in nearness with timestep for different the number densities of rays using a map with a single peak. Data points for nearness are an average of the nearness values obtained from each reconstructed map. Error bars represent one standard error.

CONCLUSIONS

A systematic method has been presented to evaluate the ability of an optical remote sensing and computed tomography system to reconstruct temporally changing concentration profiles. Fifteen different time series maps representing the generation, decay and movement of single and multiple peaks of chemicals in air were used to examine the effect on reconstruction quality of sample time, number of iterations used by the reconstruction algorithm and sampling density.

As expected, the shorter the OP-FTIR spectrometer measurement time per ray, the better the reconstructions. Minimizing overall room scan rates is critical for reconstructing concentration profiles with multiple peaks or rapidly changing concentration profiles. If shorter open-path measurement times result in a significant increase in measurement noise or error, however, longer times would provide improved image quality. Measurement time could be shortened by decreasing OP-FTIR spectrometer wavenumber resolution or the number of OP-FTIR spectrometer scans, but this will result in decreased signal to noise ratio, increased minimum detection limits for chemicals, decreased resolution of spectral features and quantification errors.

For the time series maps used in this study, scanning the entire room in 10–20 min was adequate for exposure evaluation, source monitoring and leak detection. At a timestep of 1, or 15 s per open-path measurement, the majority of reconstructed TWA exposures were within 10% of the actual exposures. A timestep of 4, or scanning the entire room in 40 min, generated maps that successfully pinpointed the location of contaminant peaks; however, peak concentrations were underestimated and artifacts were prevalent in the reconstructions. Longer sampling times resulted in concentration maps that had smeared peaks and strong artifacts related to the configuration.

In practice, the optimum sample time for an ORS-CT system will depend upon the number and type of contaminants in air, number of chemical sources, room ventilation rates, room size, purpose of the sampling program and budget. While a timestep of 2, or sampling the entire room in 20 min, was acceptable for TWA exposure evaluations, shorter sampling times will probably be required to evaluate short-term and TWA exposures accurately.

Reconstructing the simulation of a rapidly decaying gas leak using timesteps of 1 to 4 resulted in considerable overestimation of peak concentrations and maps that were filled with streaks and artifacts, although peak locations and shapes were reconstructed correctly. With this scenario, the OP-FTIR system would be adequate for leak detection; however, a faster scanning system would be required for accurate exposure assessments.

The configuration of an ORS-CT system plays a crucial role in obtaining reconstructions with good spatial resolution (Todd and Ramachandran, 1994a,b). The number of required open-path rays is related to the size, number and spatial variability of contaminant sources. For concentrations at steady state, the higher the density of open-path rays, the better the reconstructions. However, when there is significant spatial variability in concentrations over time, the requirement for accurate temporal resolution may require sampling with fewer rays to scan the room at a faster rate. Therefore, some spatial resolution will be compromised. In this study, simulations using 30 rays per OP-FTIR spectrometer resulted in better reconstructed concentration maps than simulations using 40 or 80 rays.

Optical remote sensing and computed tomography shows promise as a method to produce spatially and temporally resolved two-dimensional concentration maps of an entire room. These maps would provide near real-time visualization of contaminant generation, movement and concentrations. In this study, the simulated OP-FTIR system successfully reconstructed a variety of spatially and temporally varying time series maps using scan times that match those achievable in practice. In practice, the maps can be used for source monitoring, to track leaks and, if they are coupled with time-location information for a worker, for exposure evaluation.

Although these studies evaluated 15 different test concentration profiles, they are not representative of all possible real-life concentration profiles. Work is currently being performed in a controlled chamber, using an actual ORS-CT system, to generate time series profiles experimentally that can be used in studies developing configurations and reconstruction algorithms.

The success of an ORS-CT system will depend upon the ORS configuration, reconstruction algorithm and OP-FTIR spectrometers. The configuration is crucial because it will introduce artifacts into the reconstructions, particularly given the sparse nature of the sampling in the proposed application of tomography. In this article, the simulated ORS-CT system used a non-invasive, symmetrical four source configuration. However, in practice, the layout of rooms will place constraints on the placement of OP-FTIR spectrometers, light sources and retroreflectors. Time series concentration maps are important tools for developing this ORS-CT technology. A subsequent paper will report on using time series maps to develop ORS configurations.

Acknowledgements—This work was supported by grant K01 OH00103-01 from the National Institute for Occupational Safety and Health of the Centers for Disease Control and Prevention, by the U.S. Environmental Protection Agency cooperative agreement CR815152 with the University of North Carolina, and by the National Science Foundation (94-53433). The authors wish to thank Doug Norton for developing the computer simulation software, and Gurumurthy Ramachandran for his work on the time series program.

REFERENCES

Committee on Industrial Ventilation (1995) *Industrial Ventilation. A Manual of Recommended Practice*, 22nd edn, pp. 3–6. American Conference of Governmental Industrial Hygienists, Inc., Cincinnati, OH.

Hanna, S. R., Briggs, G. A. and Hoskar, R. P. (1982) *Handbook on Atmospheric Diffusion*. Prepared for the Office of Health and Environmental Research, U.S. Department of Energy, Technical Information Center, DOE/TIC/-11223.

Herman, G. T. (1980). Introduction. In *Image Reconstruction from Projections*. Academic Press, Inc., New York.

Rasouli, F. and Williams, T. A. (1995) Application of dispersion modeling to indoor gas release scenarios. *J. Air Waste Manage. Assoc.* **45**, 191–195.

Samanta, A. and Todd, L. (1994) Mapping chemical concentrations indoors using open-path FTIR spectroscopy and computed tomography: chamber studies. *Proc. Optical Remote Sensing Applications to Environmental and Industrial Safety Problems*, Air and Waste Management Association, McLean, VA. SPIE 2365: 187–194.

Shepp, L. A. and Vardi, Y. (1982) Maximum likelihood reconstruction for emission tomography. *IEEE Trans. Medical Imaging* **MI-1**, 113–122.

Strang, C. R. and Levine, S. P. (1989) The limits of detection for the monitoring of semiconductor manufacturing gas and vapor emissions by fourier transform infrared (FTIR) spectroscopy. *Am. ind. Hyg. Ass. J.* **50**, 78–84.

Todd, L. and Leith, D. (1990) Remote sensing and computed tomography in industrial hygiene. *Am. ind. Hyg. Ass. J.* **51**, 224–233.

Todd, L. and Ramachandran, G. (1994a) Evaluation of optical source-detector configuration for tomographic reconstruction of chemical concentrations in indoor air. *Am. ind. Hyg. Ass. J.* **55**, 1133–1143.

Todd, L. and Ramachandran, G. (1994b) Evaluation of algorithms for tomographic reconstruction of chemical concentrations in indoor air. *Am. ind. Hyg. Ass. J.* **55**, 403–417.

Tsui, B. M. W., Zhao, X., Frey, E. C. and Gulberg, G. T. (1991) Comparison between ML-EM and WLS-CG algorithms for SPECT image reconstruction. *IEEE Trans. Nucl. Sci.* **38**, 1766–1772.

Yost, M. G., Gadgil, A. J., Drescher, A. C., Zhou, Y., Simonds, M. A., Levine, S. P., Nazaroff, W. W. and Saisan, P. A. (1994) Imaging indoor tracer gas concentrations with computed tomography: experimental results with a remote sensing FTIR system. *Am. ind. Hyg. Ass. J.* **55**, 395–402.

3M Occupational Health and Environmental Safety Division (1992) 3M Organic Vapor Monitor Sampling Rate Validation Protocol No. 70-0701-3308-0(92.1).